PERGAMON

International Journal of Solids and Structures 38 (2001) 1765–1789

INTERNATIONAL JOURNAL OF SOLIDS and STRUCTURES

www.elsevier.com/locate/ijsolstr

On the modeling of integrally actuated helicopter blades

Carlos E.S. Cesnik [a,*], Sangjoon Shin [b]

[a] *Department of Aeronautics and Astronautics, Massachusetts Institute of Technology, Room 33-313, 77 Massachusetts Avenue, Cambridge, MA 02139-4307, USA*

[b] *Department of Aeronautics and Astronautics, Massachusetts Institute of Technology, Room 37-346, 70 Vassar Street, Cambridge, MA 02139, USA*

Received 17 August 1999; in revised form 7 December 1999

Abstract

This paper presents an asymptotical formulation for preliminary design of multi-cell composite helicopter rotor blades with integral anisotropic active plies. It represents the first attempt in the literature to asymptotically analyze such active structure. The analysis is broken down in two parts: a linear two-dimensional analysis over the cross-section, and a geometrically non-linear (beam) analysis along the blade span. The cross-sectional analysis revises and extends a closed form solution for thin-walled, multi-cell beams based on the variational-asymptotical method, accounting for the presence of active fiber composites distributed along the cross-section of the blade. The formulation provides expressions for the asymptotically correct cross-sectional stiffness constants in closed form, facilitating design-trend studies. These stiffness constants are then used in a beam finite element discretization of the blade reference line. This is an extension of the exact intrinsic equations for the one-dimensional analysis of rotating beams considering small strains and finite rotations, and now taking account of the presence of distributed actuators. Subject to external loads, active ply induced strains, and specific boundary conditions, the one-dimensional (beam) problem can be solved for displacements, rotations, and strains of the reference line. Analytical and numerical studies are presented to compare the proposed theory against the previously established analytical models. Discrepancies are found for general blade cross-section and discussed herein in details, especially for the piezoelectric actuation components. Direct results of the present formulation are also compared with experimental data.

Keywords: Active cross-section modeling; Embedded anisotropic actuation; Integrally twirled helicopter blades

1. Introduction

The technology of smart structures provides a new degree of design flexibility for advanced composite helicopter rotor blades. The key to the technology is the ability to allow the structure to sense and react in a desired fashion, improving rotor blade performance in the areas of structural vibration, acoustic signature, and aeroelastic stability. More specifically, there have been several approaches in the literature to take

* Corresponding author. Fax: +1-617-253-0361.
E-mail address: ccesnik@mit.edu (C.E.S. Cesnik).

0020-7683/01/$ - see front matter
PII: S0020-7683(00)00135-9

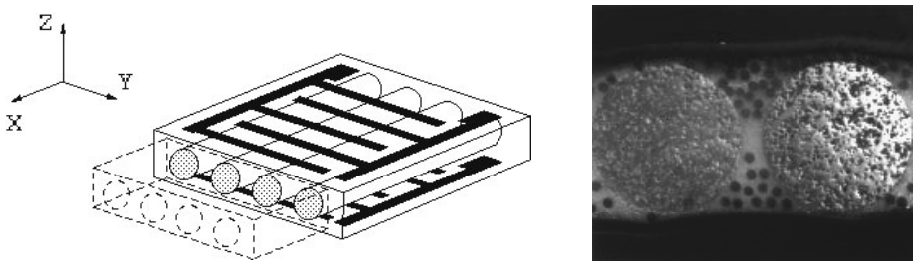

Fig. 1. Active fiber composite: (a) mode of operation, showing axial extension along fibers and contraction transverse to fibers; (b) SEM photo of the cross-section.

advantage of active materials for individual blade control (Loewy, 1997; Friedmann, 1997). The one of interest in the present work is the integral actuation through the use of anisotropic actuators, particularly through the use of active fiber composites (AFC) with interdigitated electrodes (Bent and Hagood, 1997). This actuation concept, shown in Fig. 1, provides a feasible way of integrally actuating a rotor blade instead of the direct use of piezoceramic crystals. The latter was extensively studied by Chen and Chopra (1993, 1997), following up on the work of Barrett (1990), in a 6-ft diameter two-blade Froude-scaled rotor model with banks of piezoceramic crystal elements in $\pm 45^\circ$ embedded in the upper and lower surfaces of the test blade. There have been improvements in the actuation levels by using dual-layer actuators and the maximum experimental tip twist actuation was of the order of 0.5°, still below the 1° to 2° necessary for the possible vibration control applications. On the other hand, the AFC concept obtains the level of authority needed from the actuation. Basic material characterization and proof of concept of an integral twisted-actuated rotor blade have been under investigation at MIT's Active Materials and Structures Laboratory (Rodgers et al., 1997; Cesnik et al., 1999).

In order to design and analyze those beam-like structures, an appropriate formulation is needed that takes account of the presence of embedded anisotropic actuators distributed throughout the blade in a consistent manner. Even though several approaches exist for passive blade modeling (Volovoi et al., 1999), this is not the case when one is dealing with active blades. In fact, there has been few analytical models developed so far to analyze a single-cell beam, and none for multiple-cell active beam (which is typical of helicopter blades). The most popular class of single-cell active beam model encountered in the literature is based on the passive beam structural modeling of Rehfield (1985). Examples of such are the works of Song and Librescu (1993), duPlessis and Hagood (1996), and Wilkie et al. (1996). However, since Rehfield's formulation is known to be *not* asymptotically correct (Berdichevsky et al., 1992), there is no guarantee for consistent accuracy on the results, even for the stiffness constants. Such theoretical deficiency could generate a significant discrepancy also for the actuation constants in the case of active beams. The model developed and implemented by duPlessis and Hagood (1996) is selected for this study as a representative of this class, and it is referred in this paper as *modified Rehfield model*.

The objective of this paper is to present a framework for analyzing two-cell advanced composite rotor blades with integral anisotropic active plies for designing helicopter rotor blades. It supports the joint effort between the US Army Vehicle Technology Center, at NASA Langley Center, and MIT in designing model scale active twist rotor (ATR) blades for future wind tunnel testing in the Langley Transonic Dynamics Tunnel (TDT). It also studies the discrepancies in the actuation constants arising from the modified Rehfield model-based theories and the (asymptotically correct) present formulation.

The present analysis extends the previous work done for modeling generic passive blades (Cesnik and Hodges, 1997; Hodges, 1990; Hodges et al., 1992). The approach is based on the two-step solution of the original three-dimensional blade representation by means of an asymptotical approximation: a linear two-dimensional cross-sectional analysis and a non-linear one-dimensional global analysis (Cesnik and Hodges,

1997). The resulting model is expected to correctly predict the behavior of helicopter blades, accounting for the presence of different materials (passive and active) and an approximation of the actual blade shape.

The cross-sectional analysis revises and extends the closed form solution of a thin-walled, multi-cell asymptotic formulation presented by Badir (1995). The variational-asymptotical method (Berdichevsky, 1979) is used to formulate the stiffness constants of a two-cell cross-section with the active plies consisting of piezoelectric fibers. This cross-sectional analysis is a specialized case of the general framework established in Cesnik and Hodges (1997). It provides the expressions for the asymptotically correct cross-sectional stiffness constants in closed form, facilitating design-trend studies. These stiffness constants will then be used in a beam finite element discretization of the blade reference line. The exact intrinsic equations for the one-dimensional analysis of rotating beams considering small strains and finite rotations developed by Hodges (1990) and implemented by Shang and Hodges (1995) is extended to take into account the changes in the constitutive relation. Subject to external loads, active ply induced strains, and specific boundary conditions, the one-dimensional (beam) problem can be solved for displacements, rotations, and strains of the reference line. Finally, these results could be combined with the information from the cross-sectional analysis in a set of recovering relations for stress/strain distribution at each ply of the blade. This structural representation will serve as the basis for the future aeroelastic blade design model.

2. Present formulation

2.1. Cross-section analysis

Stiffness constants for an anisotropic thin-walled two-cell beam are obtained from a variational-asymptotical formulation originally presented by Badir (1995). Herein, the original formulation is expanded to deal with active materials, the final expressions for the stiffness constants are corrected for misprints, and a validation study of such a formulation (not presented in Badir (1995)) will follow in the next section. In this section, the main steps of the cross-sectional analysis derivation are presented based on a linear beam formulation. Even though the one-dimensional (1-D) beam formulation that follows is intrinsically nonlinear, there is no loss of generality at this level to use a geometrically linear beam assumption.

Consider a slender thin-walled elastic cylindrical shell as shown in Fig. 2. It is assumed that

$$\frac{d}{L} \ll 1, \quad \frac{h}{d} \ll 1, \quad \frac{h}{R} \ll 1, \tag{1}$$

where L is length of the shell, h is thickness, $-h(s)/2 < \xi < h(s)/2$, R is the radius of curvature of the middle surface, d is a characteristic cross-section dimension, and s is defined in Fig. 2. The tangent vector $\mathbf{t}$, the normal vector $\mathbf{n}$ and the projection of the position vector $\mathbf{r}$ on $\mathbf{t}$ and $\mathbf{n}$ are expressed on the Cartesian and curvilinear coordinates as

$$\begin{aligned} \mathbf{t} &= \frac{\mathrm{d}r}{\mathrm{d}s} = \frac{\mathrm{d}y}{\mathrm{d}s}\mathbf{i}_y + \frac{\mathrm{d}z}{\mathrm{d}s}\mathbf{i}_z, \quad \mathbf{n} = \mathbf{t} \times \mathbf{i}_x = \frac{\mathrm{d}z}{\mathrm{d}s}\mathbf{i}_y - \frac{\mathrm{d}y}{\mathrm{d}s}\mathbf{i}_z, \\ r_t &= \mathbf{r} \cdot \mathbf{t} = y\frac{\mathrm{d}y}{\mathrm{d}s} + z\frac{\mathrm{d}z}{\mathrm{d}s}, \quad r_n = \mathbf{r} \cdot \mathbf{n} = y\frac{\mathrm{d}z}{\mathrm{d}s} - z\frac{\mathrm{d}y}{\mathrm{d}s}, \end{aligned} \tag{2}$$

where $\mathbf{i}_x$, $\mathbf{i}_y$, and $\mathbf{i}_z$ are unit vectors along the undeformed beam reference frame.

The energy density of a three-dimensional (3-D) elastic body is a quadratic form of the strains

$$U = \tfrac{1}{2}E^{ijkl}\varepsilon_{ij}^{(\mathrm{m})}\varepsilon_{kl}^{(\mathrm{m})}, \tag{3}$$

where the material properties are expressed by the Hookean tensor E^{ijkl}, and $i, j, k, l = 1, 2, 3$. The mechanical strain $\varepsilon_{ij}^{(\mathrm{m})}$ is the difference between the total strain ε_{ij} and the non-mechanical strain $\varepsilon_{ij}^{(\mathrm{nm})}$, i.e.

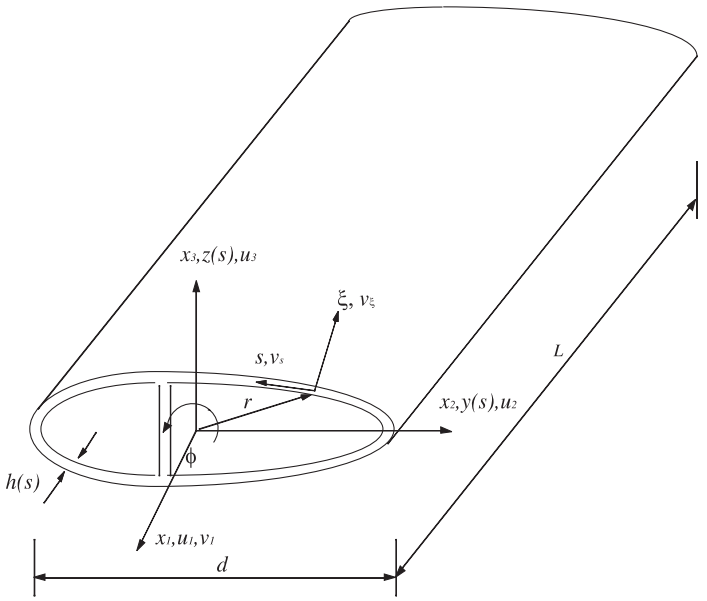

Fig. 2. Two-cell thin-walled cross-section beam.

$$\varepsilon_{ij}^{(\mathrm{m})} = \varepsilon_{ij} - \varepsilon_{ij}^{(\mathrm{nm})}, \tag{4}$$

and the total strain can be written in terms of two-dimensional (2-D) strain measures as

$$\varepsilon_{ij} = \overline{\gamma}_{ij} + \xi\rho_{ij}, \tag{5}$$

where $\overline{\gamma}_{ij}$ is in-plane strain components, and ρ_{ij} is the change in the shell surface curvature.

Considering the non-mechanical strain coming only from piezoelectric actuation, the expression of non-mechanical strain $\varepsilon_{ij}^{(\mathrm{nm})}$ from a linear piezoelectric constitutive relation (Jaffe et al., 1971) is

$$\varepsilon_{ij} = s_{ijkl}^{\mathrm{E}}\sigma_{kl} + d_{kij}E_k, \tag{6}$$

where ε_{ij} is the total strain tensor, s_{ijkl}^{E} is the elastic compliance tensor at constant electric field E_k, σ_{ij} is the stress tensor, and d_{kij} is the piezoelectric electromechanical coupling tensor. The first term in the right-hand side of Eq. (6) represents mechanical strain $\varepsilon_{ij}^{(\mathrm{m})}$, and the second one represents the non-mechanical strain, which will be denoted by $\varepsilon_{ij}^{(\mathrm{a})}$ since it results from actuation only.

The 3-D strain energy is then minimized with respect to ε_{i3} (the through-the-thickness stress components are considerably smaller than the remaining components):

$$\hat{U} = \min_{\varepsilon_{i3}} U = \tfrac{1}{2}D^{\alpha\beta\gamma\delta}\varepsilon_{\alpha\beta}^{(\mathrm{m})}\varepsilon_{\gamma\delta}^{(\mathrm{m})}, \tag{7}$$

where $D^{\alpha\beta\gamma\delta}$ is the 2-D Hookean tensor (Badir, 1995), and $\alpha, \beta, \gamma, \delta = 1, 2$.

From practical considerations, one may assume that only E_1 (electric field along the piezoelectric fibers) exists. The 2-D strain expression becomes

$$\varepsilon_{\alpha\beta}^{(\mathrm{m})} = \varepsilon_{\alpha\beta} - \varepsilon_{\alpha\beta}^{(\mathrm{a})} = \overline{\gamma}_{\alpha\beta} + \xi\rho_{\alpha\beta} - d_{1\alpha\beta}E_1. \tag{8}$$

Substitute Eq. (8) into Eq. (7) and integrate over the thickness ξ to get a shell energy Φ per unit of middle surface area

$$2\Phi = \{\langle D^{\alpha\beta\gamma\delta}\rangle\overline{\gamma}_{\alpha\beta} - 2\langle D^{\alpha\beta\gamma\delta}d_{1\gamma\delta}E_1\rangle\}\overline{\gamma}_{\gamma\delta} + 2\{\langle D^{\alpha\beta\gamma\delta}\xi\rangle\overline{\gamma}_{\alpha\beta} - \langle D^{\alpha\beta\gamma\delta}d_{1\gamma\delta}E_1\xi\rangle\}\rho_{\gamma\delta} + \langle D^{\alpha\beta\gamma\delta}\xi^2\rangle\rho_{\alpha\beta}\rho_{\gamma\delta} + \Psi(E_1), \tag{9}$$

where

$$\langle(\bullet)\rangle = \int_{-h(s)/2}^{+h(s)/2}(\bullet)\,\mathrm{d}\xi. \tag{10}$$

The function $\Psi(E_1)$ in Eq. (9) represents the quadratic terms in the electric field. Since in the actuation problem the field is prescribed, it becomes inessential in the derivation of the beam constitutive relation.

From the variational-asymptotical method (Berdichevsky, 1979), the shell energy functional after the first-order approximation is

$$2\Phi_1 = \min_{\overline{\gamma}_{22}} 2\Phi = \{A\overline{\gamma}_{11} - 2A^{(\mathrm{a})}\}\overline{\gamma}_{11} + 2B\overline{\gamma}_{11}\overline{\gamma}_{1s} + \{C\overline{\gamma}_{1s} - 2C^{(\mathrm{a})}\}\overline{\gamma}_{1s} - \Psi_2(E_1).$$

The variables A, B, and C represent the axial, coupling and shear stiffness, respectively, as described in Badir (1995), while the actuation contribution to the energy is represented by the new terms $A^{(\mathrm{a})}$, $C^{(\mathrm{a})}$, and $\Psi_2(E_1)$ as follows:

$$\begin{aligned}
A &= \langle D^{1111}\rangle - \frac{\langle D^{1122}\rangle^2}{\langle D^{2222}\rangle},\\
B &= 2\langle D^{1112}\rangle - 2\frac{\langle D^{1122}\rangle\langle D^{1222}\rangle}{\langle D^{2222}\rangle},\\
C &= 4\langle D^{1212}\rangle - 4\frac{\langle D^{1222}\rangle^2}{\langle D^{2222}\rangle},\\
A^{(\mathrm{a})} &= \langle D^{11\gamma\delta}d_{1\gamma\delta}E_1\rangle - \frac{\langle D^{1122}\rangle}{\langle D^{2222}\rangle}\langle D^{22\gamma\delta}d_{1\gamma\delta}E_1\rangle,\\
C^{(\mathrm{a})} &= 2\langle D^{12\gamma\delta}d_{1\gamma\delta}E_1\rangle - 2\frac{\langle D^{1222}\rangle}{\langle D^{2222}\rangle}\langle D^{22\gamma\delta}d_{1\gamma\delta}E_1\rangle.
\end{aligned} \tag{11}$$

Recalling that the shear flow N_{1s} is obtained as a constant and the hoop-stress resultant N_{ss} vanishes,

$$\begin{aligned}
N_{11} &= \frac{\partial\Phi_1}{\partial(\overline{\gamma}_{11})} = (A(s)\overline{\gamma}_{11} + B(s)\overline{\gamma}_{1s}) - A^{(\mathrm{a})}(s),\\
N_{1s} &= \frac{\partial\Phi_1}{\partial(2\overline{\gamma}_{1s})} = \frac{1}{2}(B(s)\overline{\gamma}_{11} + C(s)\overline{\gamma}_{1s}) - \frac{1}{2}C^{(\mathrm{a})}(s) = \text{constant}.
\end{aligned} \tag{12}$$

The warping correction function w_1 in the first-order approximation becomes

$$\frac{\partial w_1}{\partial s} = \frac{4}{C}\text{constant} - 2\frac{C}{B}u_1' + \frac{2}{C}C^{(\mathrm{a})} - u_2'\frac{\mathrm{d}y}{\mathrm{d}s} - u_3'\frac{\mathrm{d}z}{\mathrm{d}s} - \phi' r_n. \tag{13}$$

Using the single-value condition on the function w_1,

$$\oint_i \frac{\partial w_1}{\partial s}\,\mathrm{d}s = 0 \tag{14}$$

for the ith closed cell (I for first cell and II for second cell) determines the expression of the "constant" in Eqs. (12) and (13).

The displacement field relating the shell variables and the beam ones is determined as follows, which includes the warping field associated with extension $g_1(s)$, torsion $G(s)$, and bending $g_2(s)$, $g_3(s)$, respectively, as well as the displacement component directly associated with actuation, $v_1^{(a)}(s)$:

$$\begin{aligned} v_1 &= u_1(x) - y(s)u_2'(x) - z(s)u_3'(x) + G(s)\phi'(x) + g_1(s)u_1'(x) + g_2(s)u_2''(x) + g_3(s)u_3''(x) + v_1^{(a)}(s), \\ v_s &= u_2(x)\frac{dy}{ds} + u_3(x)\frac{dz}{ds} + \phi(x)r_n, \quad v_\xi = u_2(x)\frac{dz}{ds} - u_3(x)\frac{dy}{ds} - \phi(x)r_t, \end{aligned} \tag{15}$$

where

$$\begin{aligned} g_1 &= \frac{2\{(b_2+b_5)f_1 + b_2 f_2\}}{(b_1+b_2)(b_2+b_5) - b_2^2}, \qquad g_2 = \frac{2\{(b_1+b_2)f_2 + b_2 f_1\}}{(b_1+b_2)(b_2+b_5) - b_2^2}, \\ f_1 &= \oint_{\mathrm{I}} cC^{(a)}\,ds, \qquad f_2 = \oint_{\mathrm{II}} cC^{(a)}ds, \end{aligned} \tag{16}$$

$$v_1^{(a)}(s) = \begin{cases} \int_0^s \{2g_1 - C^{(a)}(\tau)\}c(\tau)\,d\tau & \text{at } s = 0 \to s_1 \text{ (left branch)}, \\ \int_0^s \{2(g_1 - g_2) - C^{(a)}(\tau)\}c(\tau)d\tau & \text{at } s = s_1 \to s_2 \text{ (web)}, \\ \int_0^s \{2g_2 - C^{(a)}(\tau)\}c(\tau)d\tau & \text{at } s = s_2 \to s_3 \text{ (right branch)} \end{cases}$$

with b_i, c defined in Appendix A, and each integral being evaluated along the corresponding branch of the two-cell cross-section. The integration subscripts I and II denote anticlockwise integration over the left and right cells, respectively (Fig. 3).

The strain field associated with Eq. (15) is

$$\begin{aligned} \bar{\gamma}_{11} &= u_1'(x) - y(s)u_2''(x) - z(s)u_3''(x), \\ 2\bar{\gamma}_{1s} &= \left(\frac{dG}{ds} + r_n\right)\phi' + \frac{dg_1}{ds}u_1' + \frac{dg_2}{ds}u_2'' + \frac{dg_3}{ds}u_3'' + \frac{dv_1^{(a)}}{ds}, \\ \bar{\gamma}_{ss} &= 0. \end{aligned} \tag{17}$$

The constitutive relations can be written in terms of stress resultants and kinematic variables by relating the traction F_1, torsional moment M_1, and bending moments M_2, M_3 to the shear flow and axial stress as follows:

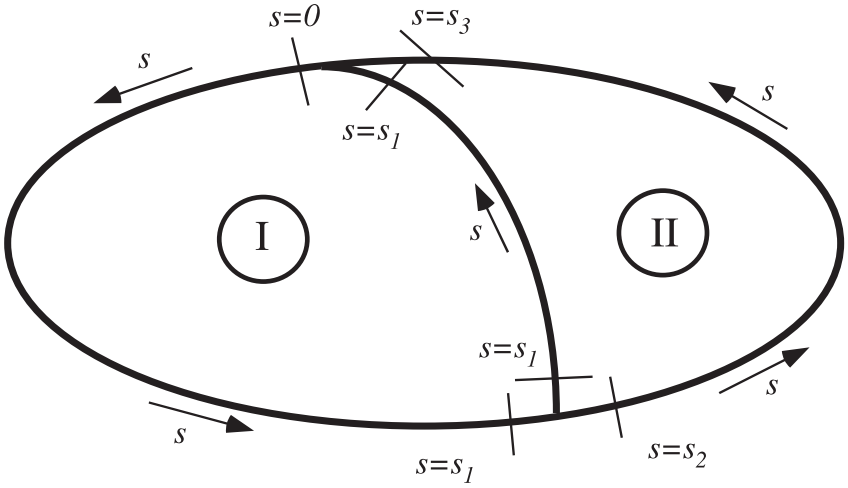

Fig. 3. Branches for integration of a two-cell thin-walled cross-section.

$$
\begin{aligned}
F_1 &= \frac{\partial \Phi_2}{\partial u_1'} = \oint \int \sigma_{11}\,\mathrm{d}\xi\,\mathrm{d}s = \oint N_{11}\,\mathrm{d}s,\\
M_1 &= \frac{\partial \Phi_2}{\partial \phi'} = \oint \int \sigma_{1s} r_n(s)\mathrm{d}\xi\,\mathrm{d}s = \oint N_{1s} r_n(s)\mathrm{d}s,\\
M_2 &= \frac{\partial \Phi_2}{\partial(-u_3'')} = \oint \int \sigma_{11} z(s)\mathrm{d}\xi\,\mathrm{d}s = \oint N_{11} z(s)\mathrm{d}s,\\
M_3 &= \frac{\partial \Phi_2}{\partial u_2''} = -\oint \int \sigma_{11} y(s)\mathrm{d}\xi\,\mathrm{d}s = -\oint N_{11} y(s)\mathrm{d}s.
\end{aligned}
\tag{18}
$$

Substituting Eqs. (12) and (18) into the first equation in Eq. (18), one gets

$$
\begin{aligned}
F_1 &= \oint N_{11}\mathrm{d}s = \oint \{A\overline{\gamma}_{11} + B\overline{\gamma}_{1s} - A^{(\mathrm{a})}\}\mathrm{d}s\\
&= \oint \left[A\{u_1' - y u_2'' - z u_3''\} + \frac{1}{2}\left\{ \left(\frac{\mathrm{d}G}{\mathrm{d}s} + r_n\right)\phi' + \frac{\mathrm{d}g_1}{\mathrm{d}s}u_1' + \frac{\mathrm{d}g_2}{\mathrm{d}s}u_2'' + \frac{\mathrm{d}g_3}{\mathrm{d}s}u_3'' + \frac{\mathrm{d}v_1^{(\mathrm{a})}}{\mathrm{d}s} \right\} - A^{(\mathrm{a})} \right]\mathrm{d}s\\
&= K_{11}u_1' + K_{12}\phi' + K_{13}u_3'' + K_{14}u_2'' + \oint \left(\frac{B}{2}\frac{\mathrm{d}v_1^{(\mathrm{a})}}{\mathrm{d}s} - A^{(\mathrm{a})} \right)\mathrm{d}s
\end{aligned}
\tag{19}
$$

and similarly with the other three moment equations. The first four terms in the final part of the right-hand side of Eq. (19) correspond to the stiffness coefficients for an anisotropic two-cell beam. (Detailed expressions of K_{ij} and relevant parameters are given in Appendix A.) The last term (following those) results from piezoelectric actuation and can be regarded as a forcing component. The general form of the constitutive relation can be written as

$$
\begin{Bmatrix} F_1 \\ M_1 \\ M_2 \\ M_3 \end{Bmatrix} = \begin{bmatrix} K_{11} & K_{12} & K_{13} & K_{14} \\ K_{12} & K_{22} & K_{23} & K_{24} \\ K_{13} & K_{23} & K_{33} & K_{34} \\ K_{14} & K_{24} & K_{34} & K_{44} \end{bmatrix} \cdot \begin{Bmatrix} u_1' \\ \phi' \\ -u_3'' \\ u_2'' \end{Bmatrix} - \begin{Bmatrix} F_1^{(\mathrm{a})} \\ M_1^{(\mathrm{a})} \\ M_2^{(\mathrm{a})} \\ M_3^{(\mathrm{a})} \end{Bmatrix}.
\tag{20}
$$

Explicit expressions of piezoelectric actuation contributing to the constitute relation are given by

$$
\begin{aligned}
F_1^{(\mathrm{a})} &= \oint \left\{ A^{(\mathrm{a})} - \frac{B}{C}C^{(\mathrm{a})} \right\}\mathrm{d}s + 2g_1 \oint_{\mathrm{I}} \frac{B}{C}\,\mathrm{d}s + 2g_2 \oint_{\mathrm{II}} \frac{B}{C}\,\mathrm{d}s,\\
M_1^{(\mathrm{a})} &= -2g_1 A_{e\mathrm{I}} - 2g_2 A_{e\mathrm{II}},\\
M_2^{(\mathrm{a})} &= -\oint \left\{ A^{(\mathrm{a})} - \frac{B}{C}C^{(\mathrm{a})} \right\} z\,\mathrm{d}s - 2g_1 \oint_{\mathrm{I}} \frac{B}{C} z\,\mathrm{d}s - 2g_2 \oint_{\mathrm{II}} \frac{B}{C} z\,\mathrm{d}s,\\
M_3^{(\mathrm{a})} &= \oint \left\{ A^{(\mathrm{a})} - \frac{B}{C}C^{(\mathrm{a})} \right\} y\,\mathrm{d}s + 2g_1 \oint_{\mathrm{I}} \frac{B}{C} y\,\mathrm{d}s + 2g_2 \oint_{\mathrm{II}} \frac{B}{C} y\,\mathrm{d}s,
\end{aligned}
\tag{21}
$$

where integral without any subscripts $\oint$ denotes over-all-section evaluation, which is a summation of evaluations over $s = 0 \to s_1$, $s = s_1 \to s_2$ and $s = s_2 \to s_3$.

2.2. 1-D Beam analysis

A non-linear one-dimensional global analysis considering small strains and finite rotations is proposed here as a direct expansion of the mixed variational intrinsic formulation of moving beams originally

presented by Hodges (1990), and implemented by Shang and Hodges (1995). The notation used in this section is based on matrix notation to be consistent with the original derivation. The main steps of the formulation are repeated here, and emphasis is given at the points where the effects of the active material embedded in the structure change the equations.

As shown in Fig. 4, a global frame denoted a is rotating with the rotor, with its triad axes labeled as a_1, a_2 and a_3. The undeformed reference frame of the blade is denoted b, with its axes labeled as b_1, b_2 and b_3, and the deformed reference frame denoted B, with its axes labeled as B_1, B_2 and B_3, though not shown in the figure. Any arbitrary vector represented by its components in one of the basis may be converted to another basis by using appropriate transformation matrices. For example, C^{ba} is the transformation matrix from a to b, and C^{Ba} is that from a to B. There are several ways to express the transformation matrices. C^{ba} can be expressed in terms of direction cosines from the initial geometry of the rotor blade, while C^{Ba} contains the unknown rotation variables.

As described in detail in Hodges (1990), the variational formulation is derived from Hamilton's principle which can be written as

$$\int_{t_1}^{t_2}\int_0^l [\delta(K-U)+\overline{\delta W}]\mathrm{d}x_1\mathrm{d}t = \overline{\delta \mathsf{A}}, \tag{22}$$

where t_1 and t_2 are arbitrarily fixed times, K and U are the kinetic and potential energy densities per unit span, respectively. $\overline{\delta \mathsf{A}}$ is the virtual action at the ends of the beam and at the ends of the time interval, and $\overline{\delta W}$ is the virtual work of applied loads per unit span.

Taking the variation of the kinetic and potential energy terms with respect to γ and κ, one gets the generalized strain column vectors, and with respect to V_B and Ω_B, the linear and angular velocity column vectors:

$$F_B = \left(\frac{\partial U}{\partial \gamma}\right)^T, \qquad M_B = \left(\frac{\partial U}{\partial \kappa}\right)^T, \qquad P_B = \left(\frac{\partial K}{\partial V_B}\right)^T, \qquad H_B = \left(\frac{\partial K}{\partial \Omega_B}\right)^T, \tag{23}$$

where F_B and M_B are internal force and moment column vectors, and P_B and H_B are linear and angular momentum column vectors.

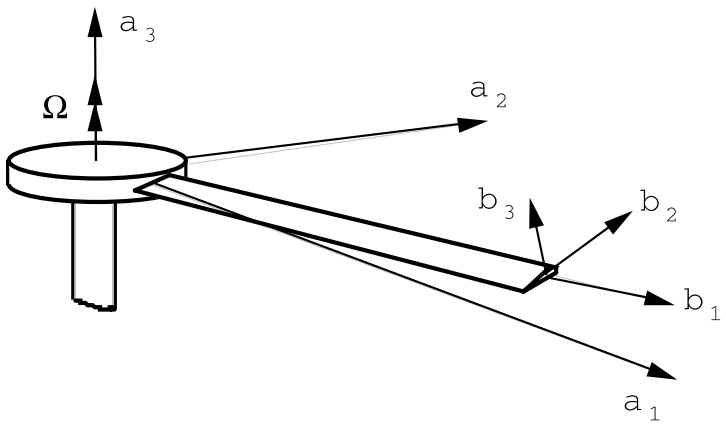

Fig. 4. Global blade frames of reference.

The geometrical exact kinematical relations in the a frame are given by

$$\begin{aligned}
\gamma^* &= C^{\mathrm{Ba}}(C^{\mathrm{ab}}e_1 + u_{\mathrm{a}}') - e_1,\\
\kappa^* &= C^{\mathrm{ba}}\left(\frac{\Delta - \frac{\widetilde{\theta}}{2}}{1+\frac{\theta^{\mathrm{T}}\theta}{4}}\right)\theta',\\
V_{\mathrm{B}}^* &= C^{\mathrm{Ba}}(v_{\mathrm{a}} + \dot{u}_{\mathrm{a}} + \widetilde{\omega}_{\mathrm{a}}u_{\mathrm{a}}),\\
\Omega_{\mathrm{B}}^* &= C^{\mathrm{ba}}\left(\frac{\Delta - \frac{\widetilde{\theta}}{2}}{1+\frac{\theta^{\mathrm{T}}\theta}{4}}\right)\dot{\theta} + C^{\mathrm{Ba}}\omega_{\mathrm{a}},
\end{aligned} \tag{24}$$

where u_{a} is the displacement vector measured in the a frame, θ is the rotation vector expressed in terms of Rodrigues parameters, e_1 is the unit vector $[1,0,0]^{\mathrm{T}}$, Δ is the 3×3 identity matrix, v_{a} and w_{a} are the initial velocity and initial angular velocity of a generic point on the a frame. The $\widetilde{(\ )}$ operator applied to a column vector is defined as

$$\widetilde{Z} = \begin{bmatrix} 0 & -Z_3 & Z_2 \\ Z_3 & 0 & -Z_1 \\ -Z_2 & Z_1 & 0 \end{bmatrix}.$$

To form a mixed formulation, Lagrange multipliers are used to enforce V_{B}, Ω_{B}, γ and κ to satisfy the geometric equations in Eq. (24).

Manipulating the equations accordingly (Shang and Hodges, 1995), one can obtain the a frame version of the variational formulation based on an exact intrinsic equations for dynamics of moving beams as

$$\int_{t_1}^{t_2} \delta\Pi_{\mathrm{a}}\,\mathrm{d}t = 0, \tag{25}$$

where

$$\begin{aligned}
\delta\Pi_{\mathrm{a}} = \int_0^l \Bigg\{ & \delta u_{\mathrm{a}}'^{\mathrm{T}} C^{\mathrm{T}}C^{\mathrm{ab}}F_{\mathrm{B}} + \delta u_{\mathrm{a}}^{\mathrm{T}}\left[\left(C^{\mathrm{T}}C^{\mathrm{ab}}P_{\mathrm{B}}\right)^{\bullet} + \widetilde{\omega}_{\mathrm{a}}C^{\mathrm{T}}C^{\mathrm{ab}}P_{\mathrm{B}}\right] + \overline{\delta\psi}_{\mathrm{a}}'^{\mathrm{T}}C^{\mathrm{T}}C^{\mathrm{ab}}M_{\mathrm{B}} - \overline{\delta\psi}_{\mathrm{a}}^{\mathrm{T}}C^{\mathrm{T}}C^{\mathrm{ab}}(\widetilde{e_1}+\widetilde{\gamma})F_{\mathrm{B}}\\
& + \overline{\delta\psi}_{\mathrm{a}}^{\mathrm{T}}\left[\left(C^{\mathrm{T}}C^{\mathrm{ab}}H_{\mathrm{B}}\right)^{\bullet} + \widetilde{\omega}_{\mathrm{a}}C^{\mathrm{T}}C^{\mathrm{ab}}H_{\mathrm{B}} + C^{\mathrm{T}}C^{\mathrm{ab}}\widetilde{V}_{\mathrm{B}}P_{\mathrm{B}}\right] - \overline{\delta F}_{\mathrm{a}}^{\mathrm{T}}\left[C^{\mathrm{T}}C^{\mathrm{ab}}(e_1+\gamma) - C^{\mathrm{ab}}e_1\right]\\
& - \overline{\delta F}_{\mathrm{a}}'^{\mathrm{T}}u_{\mathrm{a}} - \overline{\delta M}_{\mathrm{a}}^{\mathrm{T}}\left(\Delta + \frac{\widetilde{\theta}}{2} + \frac{\theta\theta^{\mathrm{T}}}{4}\right)C^{\mathrm{ab}}\kappa - \overline{\delta M}_{\mathrm{a}}'\theta + \overline{\delta P}_{\mathrm{a}}^{\mathrm{T}}\left(C^{\mathrm{T}}C^{\mathrm{ab}}V_{\mathrm{B}} - v_{\mathrm{a}} - \widetilde{\omega}_{\mathrm{a}}u_{\mathrm{a}}\right)\\
& - \overline{\delta P}_{\mathrm{a}}^{\mathrm{T}}\dot{u}_{\mathrm{a}} + \overline{\delta H}_{\mathrm{a}}^{\mathrm{T}}\left(\Delta - \frac{\widetilde{\theta}}{2} + \frac{\theta\theta^{\mathrm{T}}}{2}\right)\left(C^{\mathrm{T}}C^{\mathrm{ab}}\Omega_{\mathrm{B}} - \omega_{\mathrm{a}}\right) - \overline{\delta H}_{\mathrm{a}}^{\mathrm{T}}\dot{\theta} - \delta u_{\mathrm{a}}^{\mathrm{T}}f_{\mathrm{a}} - \overline{\delta\psi}_{\mathrm{a}}^{\mathrm{T}}m_{\mathrm{a}}\Bigg\}\mathrm{d}x_1\\
& - \left|\left(\delta u_{\mathrm{a}}^{\mathrm{T}}F_{\mathrm{a}} + \overline{\delta\psi}_{\mathrm{a}}^{\mathrm{T}}M_{\mathrm{a}} - \overline{\delta F}_{\mathrm{a}}^{\mathrm{T}}u_{\mathrm{a}} - \overline{\delta M}_{\mathrm{a}}^{\mathrm{T}}\theta\right)\right|_0^l
\end{aligned} \tag{26}$$

and the rotation matrix C is the product $C^{\mathrm{ab}}C^{\mathrm{Ba}}$ and can be expressed in terms of θ as

$$C = \frac{\left(1-\frac{\theta^{\mathrm{T}}\theta}{4}\right)\Delta - \widetilde{\theta} + \frac{\theta\theta^{\mathrm{T}}}{2}}{1+\frac{\theta^{\mathrm{T}}\theta}{4}}. \tag{27}$$

In Eq. (26), f_{a} and m_{a} are the external forces and moment vectors, respectively, which result from aerodynamics loads. The $(\ )^{\bullet}$ means derivative with respect to time. The generalized strain and force measures, and velocity and momentum measures are related through the constitutive relations in the following form:

$$\begin{Bmatrix} F_B \\ M_B \end{Bmatrix} = [K]\begin{Bmatrix} \gamma \\ \kappa \end{Bmatrix} - \begin{Bmatrix} F_B^{(a)} \\ M_B^{(a)} \end{Bmatrix}, \quad \begin{Bmatrix} P_B \\ H_B \end{Bmatrix} = \begin{bmatrix} m\Delta & 0 \\ 0 & I \end{bmatrix}\begin{Bmatrix} V_B \\ \Omega_B \end{Bmatrix} \tag{28}$$

and these expressions are solved for γ, κ, V_B, and Ω_B as function of the other measures and constants and used in Eq. (26). The stiffness $[K]$ is in general a 6×6 matrix, function of material distribution and cross-sectional geometry. As described in Hodges et al. (1992), the 6×6 stiffness matrix is related to the 4×4 one. The latter is used in this paper, where the stiffness matrix and column vector for the piezoelectric actuation are described by Eq. (20).

Adopting a finite element discretization by dividing the blade into N elements, Eq. (25) is written as

$$\int_{t_1}^{t_2} \sum_i \delta\Pi_i \, dt = 0, \tag{29}$$

where index i indicates the ith element with length Δl_i, $\delta\Pi_i$ is the corresponding spatial integration of the function in Eq. (31) over the ith element. Due to the formulation's weakest form, the simplest shape functions can be used. Therefore, the following transformation and interpolation are applied within each element (Shang and Hodges, 1995):

$$x = x_i + \xi\Delta l_i, \quad dx = \Delta l_i \, d\xi, \quad (\ )' = \frac{1}{\Delta l_i}\frac{d}{d\xi}(\ ), \tag{30}$$

$$\begin{aligned}
\delta u_a &= \delta u_i(1-\xi) + \delta u_{i+1}\xi, \quad u_a = u_i, \\
\overline{\delta\psi}_a &= \overline{\delta\psi}_i(1-\xi) + \overline{\delta\psi}_{i+1}\xi, \quad \theta = \theta_i, \\
\overline{\delta F}_a &= \overline{\delta F}_i(1-\xi) + \overline{\delta F}_{i+1}\xi, \quad F_B = F_i, \\
\overline{\delta M}_a &= \overline{\delta M}_i(1-\xi) + \overline{\delta M}_{i+1}\xi, \quad M_B = M_i, \\
\overline{\delta P}_a &= \overline{\delta P}_i, \quad P_B = P_i, \\
\overline{\delta H}_a &= \overline{\delta H}_i, \quad H_B = H_i,
\end{aligned}$$

where u_i, θ_i, F_i, M_i, P_i and H_i are constant vectors at each node i, and all δ quantities are arbitrary. ξ varies from 0 to 1.

With these shape functions, the spatial integration in Eq. (29) can be performed explicitly to give

$$\begin{aligned}
&\sum_{i=1}^{N} \Big\{ \delta u_i^T f_{u_i} + \overline{\delta\psi}_i^T f_{\psi_i} + \overline{\delta F}_i^T f_{F_i} + \overline{\delta M}_i^T f_{M_i} + \overline{\delta P}_i^T f_{P_i} + \overline{\delta H}_i^T f_{H_i} + \delta u_{i+1}^T f_{u_{i+1}} \\
&\qquad + \overline{\delta\psi}_{i+1}^T f_{\psi_{i+1}} + \overline{\delta F}_{i+1}^T f_{F_{i+1}} + \overline{\delta M}_{i+1}^T f_{M_{i+1}} \Big\} \\
&\quad = \delta u_{N+1}^T \hat{F}_{N+1} + \overline{\delta\psi}_{N+1}^T \hat{M}_{N+1} - \overline{\delta F}_{N+1}^T \hat{u}_{N+1} - \overline{\delta M}_{N+1}^T \hat{\theta}_{N+1} - \delta u_1^T \hat{F}_1 - \overline{\delta\psi}_1^T \hat{M}_1 + \overline{\delta F}_1^T \hat{u}_1 - \overline{\delta M}_1^T \hat{\theta}_1,
\end{aligned} \tag{31}$$

where the f_{u_i}, $f_{\psi_i}, \ldots, f_{M_{i+1}}$ are the element functions explicitly integrated from the formulation and described explicitly in Appendix A.

In each element function, γ and κ should be replaced with a form that is a function of F_B and M_B using the inverse form of Eq. (28), along with the piezoelectric forcing vector $F_B^{(a)}$ and $M_B^{(a)}$. So does V_B and Ω_B with a form about P_B and H_B. Detailed expressions of the element functions in Eq. (32) are shown in Appendix A with the changes caused by the presence of actuators embedded in the structure.

Since each δ-quantity is arbitrary, Eq. (32) yields a group of equations that can be written in operator form as

$$G(X, \dot{X}, \bar{F}) = 0, \tag{32}$$

where X is the column matrix of unknowns and G is a column matrix of functions. $\bar{F}$ is a column matrix containing the external nodal loads. Both X and G are of dimension $18N + 12$, in the case of a cantilever beam.

The solutions of interest of Eq. (32) can be expressed as a combination of two components:

$$X = \bar{X} + \check{X}(t), \tag{33}$$

where $\bar{X}$ represents the steady component, which is independent of time, and $\check{X}(t)$ is the transient components of the solution, or, the perturbed motion, which contains the time dependency.

In the steady state, $\check{X}(t) = 0$, and Eq. (32) becomes

$$G(\bar{X}, 0, \bar{F}) = 0 \tag{34}$$

or simply,

$$G(\bar{X}, \bar{F}) = 0. \tag{35}$$

Following the solution procedure for the non-linear equation adopted in Shang and Hodges (1995), the use of the Newton–Raphson method requires gradient information. The Jacobian matrix can be derived explicitly by differentiation:

$$[J] = \left[\frac{\partial G}{\partial \bar{X}}\right] \tag{36}$$

leading to a very sparse matrix, that enables an efficient calculation of the solution. Note that the presence of actuation on the blade changes the original terms of the Jacobian in a similar manner it does in Eq. (32).

The solution from the 1-D beam analysis provides blade displacement and generalized stress fields due to external loading and piezoelectric actuation, which are of interest in the analysis of static and dynamic deformations, dynamic stability, and aeroelastic stability.

3. Analytical study on actuation constants

3.1. Reduction of actuation formulation

The present two-cell cross-section model yields the constitutive relation based on a 4×4 stiffness matrix and an additional column vector associated with the actuation effects as in Eq. (20). The formulation adopted in the modified Rehfield model is based on a 7×7 stiffness matrix, where (two) transverse shear and restrained warping degrees of freedom are explicitly added to the four classical degrees of freedom. Therefore, a consistent condensation to a 4×4 matrix is necessary for a meaningful comparison between them. This condensation is implemented through minimization of the potential energy with respect to the extra degrees of freedom as described, for example, in Hodges et al. (1992). A 7×1 actuation vector can be reduced to a 4×1 representation in a similar procedure. The analytical reduction procedure on the modified Rehfield model results in reasonably complex expressions for the actuation components. The 4×4 based expressions of both theories are presented in Table 1, and the reduced equations for the modified Rehfield method is based on the assumption of a beam without twist-shear coupling. Also, the nomenclature used in each expression is identified and substituted with common symbols. As a result, one can directly compare the four components of the actuation vector for the case of a single-cell active beam.

As an example of the derivation of the results presented on Table 1, consider the actuation twist moment, $M_1^{(a)}$ (remaining actuation components can be treated similarly). The expression for $M_1^{(a)}$ in the modified Rehfield's single-cell beam model is as follows (duPlessis and Hagood (1996)):

Table 1
Analytical expressions of the actuation components for single-cell active beam

$F_1^{(a)}$	Present	$\oint A^{(a)}\,ds - \oint \frac{B}{C} C^{(a)}\,ds + \left(\oint \frac{B}{C}\,ds / \oint \frac{1}{C}\,ds\right) \oint \frac{1}{C} C^{(a)}\,ds$
	Modified Rehfield	$\oint A^{(a)}\,ds - \left(\oint C\left(\frac{\partial v}{\partial s}\right) ds / \oint C\left(\frac{\partial v}{\partial s}\right)^2 ds\right) \oint C^{(a)}\left(\frac{\partial v}{\partial s}\right) ds - \left(\oint C\left(\frac{\partial z}{\partial s}\right) ds / \oint C\left(\frac{\partial z}{\partial s}\right)^2 ds\right) \oint C^{(a)}\left(\frac{\partial z}{\partial s}\right) ds$
$M_1^{(a)}$	Present	$\left(\oint \frac{1}{C} C^{(a)}\,ds / \oint \frac{1}{C}\,ds\right) A_e$
	Modified Rehfield	$\left(\oint \frac{1}{G_{\text{eff}}} C^{(a)}\,ds / \oint \frac{1}{G_{\text{eff}}}\,ds\right) A_e$
$M_2^{(a)}$	Present	$\oint A^{(a)} z\,ds - \oint \frac{B}{C} C^{(a)} z\,ds + \left(\oint \frac{B}{C} z\,ds / \oint \frac{1}{C}\,ds\right) \oint \frac{1}{C} C^{(a)}\,ds$
	Modified Rehfield	$\oint A^{(a)} z\,ds + \oint \left\{\langle \xi D^{11\gamma\delta} d_{1\gamma\delta} E_1\rangle - \left(\langle \xi D^{22\gamma\delta} d_{1\gamma\delta} E_1\rangle / \langle D^{2222}\rangle\right)\right\} \left(\frac{\partial y}{\partial s}\right) ds$
$M_3^{(a)}$	Present	$-\oint A^{(a)} y\,ds + \oint \frac{B}{C} C^{(a)} y\,ds - \left(\oint \frac{B}{C} y\,ds / \oint \frac{1}{C}\,ds\right) \oint \frac{1}{C} C^{(a)}\,ds$
	Modified Rehfield	$-\oint A^{(a)} y\,ds + \oint \left\{\langle \xi D^{11\gamma\delta} d_{1\gamma\delta} E_1\rangle - \left(\langle \xi D^{22\gamma\delta} d_{1\gamma\delta} E_1\rangle / \langle D^{2222}\rangle\right)\right\} \left(\frac{\partial z}{\partial s}\right) ds$

$$M_{1\,\text{Rehfield}}^{(a)} = \oint_\Gamma (N_{1s}^{(a)})^* \left(-\frac{2A\alpha}{\Gamma}\right) ds = \frac{\oint_\Gamma (N_{1s}^{(a)})^* \frac{1}{G_{\text{eff}} t}\,ds}{\oint_\Gamma \frac{1}{G_{\text{eff}} t}\,ds} (-2A), \tag{37}$$

where Γ represents the cross-section contour as well as the actual mid-plane contour length of the single cell, and

$$(N_{1s}^{(a)})^* = N_{1s}^{(a)} - \frac{A_{26}}{A_{22}} N_{ss}^{(a)}, \quad N_{1s}^{(a)} = \langle D^{1s\gamma\delta} d_{1\gamma\delta} E_1\rangle, \quad N_{ss}^{(a)} = \langle D^{ss\gamma\delta} d_{1\gamma\delta} E_1\rangle. \tag{38}$$

The effective shear stiffness G_{eff} is defined as follows (Smith and Chopra, 1990):

$$G_{\text{eff}} = h(s) \left(A'_{66} - \frac{(A'_{16})^2}{A'_{11}}\right), \quad A'_{11} = A_{11} - \frac{(A_{12})^2}{A_{22}},\ A'_{16} = A_{16} - \frac{A_{12} A_{26}}{A_{22}},\ A'_{66} = A_{66} - \frac{(A_{26})^2}{A_{22}}, \tag{39}$$

where A_{ij} corresponds to the elements in $[A]$ derived from the classical laminated plate theory (Jones, 1975).

On the other hand, the expression of $M_1^{(a)}$ corresponding to the single-cell cross-section from the present model can be derived as follows:

$$M_{1\,\text{present}}^{(a)} = -2g_1 A_{e\text{I}} - 2g_2 A_{e\text{II}} = -g_1 \oint_{\text{I}} r_n\,ds - g_2 \oint_{\text{II}} r_n\,ds.$$

In case of single-cell cross-section, $b_2 \to \infty$ since the integral over the web ($s = s_1 \to s_2$) vanishes. Therefore, from the definition of g_1 and g_2 in Eq. (16),

$$g_1 = 2\frac{f_1 + f_2}{b_1 + b_5}, \qquad g_2 = 2\frac{f_1 + f_2}{b_1 + b_5},$$

one gets

$$M_{1\,\text{present}}^{(a)} = -2\frac{f_1 + f_2}{b_1 + b_5}\left[\int_0^{s_1} r_n\,ds + \int_{s_2}^{s_3} r_n\,ds\right] = -2\frac{\oint_\Gamma \frac{C^{(a)}}{C}\,ds}{\oint_\Gamma \frac{1}{C}\,ds} \oint_\Gamma r_n\,ds. \tag{40}$$

Comparing both expressions, Eq. (37) and Eq. (40), the corresponding elements are equivalent to one another. That is, $(-2A)$ in Eq. (37) is equivalent to $-2\oint_\Gamma r_n\,ds$ in Eq. (40) for a single-cell cross-section. From the definition of $C^{(a)}$ (Eq. (11)), the integral in the first term leads to

$$\langle D^{12\gamma\delta} d_{1\gamma\delta} E_1\rangle = \langle \{D^{1211} d_{111} + D^{1212} d_{112} + D^{1221} d_{121} + D^{1222} d_{122}\} E_1\rangle,$$

which is equivalent to $N_{1s}^{(a)}$ and so does $\langle D^{22\gamma\delta} d_{3\gamma\delta} E_3\rangle$ to $N_{ss}^{(a)}$. Therefore, $C^{(a)}$ in Eq. (40) is equivalent to $2\,(N_{1s}^{(a)})^*$ in Eq. (37). Finally, the comparable expressions for $M_1^{(a)}$ from both models result in

$$M_{1\,\text{Rehfield}}^{(a)} = \frac{\oint \frac{1}{G_{\text{eff}}} C^{(a)} ds}{\oint \frac{1}{G_{\text{eff}}}\,ds} A_e, \quad M_{1\,\text{present}}^{(a)} = \frac{\oint \frac{1}{C} C^{(a)} ds}{\oint \frac{1}{C}\,ds} A_e. \tag{41}$$

As one can see, the form of the equations is the same, and the difference lies on the definitions of C and G_{eff}. From Eq. (11),

$$C = 4\langle D^{1212}\rangle - 4\frac{\langle D^{1222}\rangle^2}{\langle D^{2222}\rangle} = A_{66} - \frac{(A_{26})^2}{A_{22}}. \tag{42}$$

Comparing Eq. (42) with Eq. (39), C corresponds to the first term of G_{eff} by its definition and this already indicates a discrepancy between the two models. This is the same problem found with Rehfield's model for the torsional stiffness term (Berdichevsky et al., 1992). An overall analysis of these discrepancies is carried out in details in the next section.

3.2. Analytical examination of actuation components

As one can see from Table 1, the expressions do not coincide in general and this can be attributed in large by the different (out-of-plane) warping functions used in the two formulations (inplane warping became negligible due to the thin-walled assumption). Rehfield (1985) uses an ad hoc warping function, while the present asymptotical method calculates it from the basic original shell statement. Discussion of the difference in the warping function between the asymptotical formulation and others, including Rehfield (1985), can be found in Berdichevsky et al. (1992). However, for certain configurations, the difference vanishes and the formulations coincide. This is definitely the case for isotropic beams, where all the terms are identical. For $F_1^{(a)}$, the leading term is the same, but the two following ones are totally different. The terms in the present approach comes from the effects of warping associated with extension. The terms in the modified Rehfield are associated with the extension-shear coupling. So, all those terms will vanish and the results coincide when there is no extension-shear coupling present in the lay-ups ($B \equiv 0$). For $M_1^{(a)}$, the two expressions will coincide when the beam has constant stiffness and thickness along its cross-section circumference (then $C \equiv G_{\text{eff}}$). Finally, for $M_2^{(a)}$ and $M_3^{(a)}$, the leading terms are identical, but the remaining ones are totally different in nature. The second integral on the modified Rehfield method comes from an attempt to introduce ad hoc corrections due to thickness effects (thick-wall effects – duPlessis and Hagood, 1996), and it will not be considered in this comparison. The two other terms in the present formulation come from the warping associated effects, and there are two situations when they will disappear from the formulation: (i) there is no extension-shear coupling ($B \equiv 0$); and/or (ii) the beam has a constant stiffness (including the active layers) and thickness distribution along the cross-section circumference. As one can see, for a generic lay-up, the popular Rehfield-based models will present qualitative discrepancies from the asymptotically correct one. The level of impact of such discrepancies can only be quantified numerically.

4. Numerical results

In order to validate the formulation, a verification process is carried out in each step of the development. The numerical results are divided as follows:

- two-cell box beam, which numerically validates the stiffness constants of the passive multi-cell beam formulation;
- single-cell active beam, which provides numerical and experimental comparisons for both the stiffness constants and the actuation constants, and also shows the trend of discrepancies between actuation constants calculated from the different models;
- one-sixth Mach-scaled two-cell CH-47D active blade, which provides experimental results of a realistic active helicopter blade for comparison with the present formulation.

4.1. Two-cell box beam

The formulation for the passive stiffness coefficients for an anisotropic two-cell beam used here was first derived in Badir (1995). However, the author does not validate the closed-form results presented there. So, after rederiving and making corrections to the stiffness constants expressions, numerical tests were performed for two-cell beams without piezoelectric actuators. The present results are then compared with the ones from variational-asymptotical beam section analysis (VABS) (Cesnik and Hodges, 1997), a more general asymptotically-correct finite-element-based cross-sectional analysis intended for modeling generic geometries (including multiple-cell), which has been validated extensively (Volovoi et al., 1999).

As an example, consider the two cell box beam configuration represented in Fig. 5, the material properties of which are given in Table 2. VABS was run with the cross-section being discretized with 364 six-node isoparametric elements for a total of 909 nodes.

A comparison of the stiffness coefficients from both theories is provided in Table 3. The present formulation is in good agreement with VABS, with the errors well within the difference expected for this kind of thin-walled cross-sectional formulation (Cesnik and Hodges, 1997). Results for other cross-sections could be shown, but the conclusion will be similar to this one due to the nature of the asymptotical formulation. The limiting assumption is that the thickness of the wall compared to the cross-sectional characteristic dimension must be small when compared to unit.

4.2. Single-cell active beam

For a preliminary assessment of the piezoelectric actuation change in the constitutive relation, results from the present formulation are compared against the modified Rehfield model duPlessis and Hagood (1996).

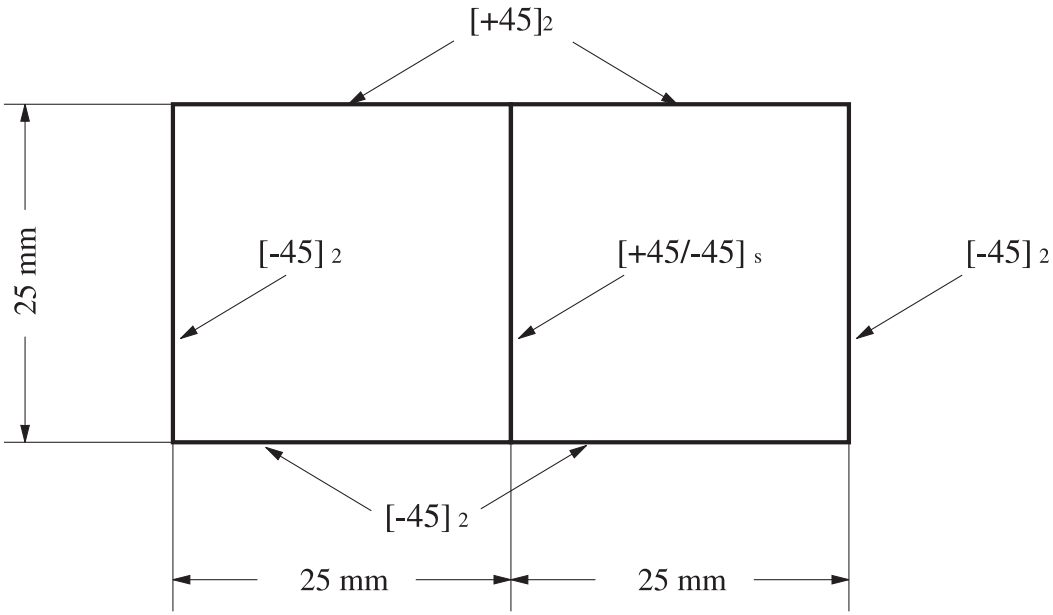

Fig. 5. Two-cell thin-walled box beam definition.

Table 2
Properties of AS4/3506-1 graphite/epoxy – "L" direction is along the fibers, "T" direction is transverse to the fibers, and "N" is normal to laminate

$E_{LL} = 142$ GPa
$E_{NN} = E_{TT} = 9.8$ GPa
$G_{LT} = G_{LN} = 6.0$ GPa
$G_{TN} = 4.80$ GPa
$\nu_{LT} = \nu_{LN} = 0.3$
$\nu_{TN} = 0.42$
Ply thickness = 0.127 mm

Table 3
Non-zero stiffness results (N, N m, N m^2) for two-cell box beam (1, extension; 2, torsion; 3, 4, bending)

K_{ij}	Present	VABS	Difference (%)
K_{11}	8.472×10^5	8.477×10^5	−0.1
K_{12}	-1.828×10^3	-1.794×10^3	+1.9
K_{13}	6.395×10^2	6.337×10^2	+0.9
K_{22}	1.299×10^2	1.278×10^2	+1.6
K_{23}	4.547×10^1	4.461×10^1	−1.9
K_{33}	9.631×10^1	9.567×10^1	+0.7
K_{44}	2.075×10^2	2.070×10^2	+0.2

The test case chosen is an airfoil-shaped cross-section with piezoelectric actuators attached at the upper and lower surfaces. This is one of the model beams fabricated and tested by duPlessis and Hagood (1996) using active fiber composites. In each pack of AFC, the piezoelectric (PZT-5H) fibers are aligned in +45° in order to maximize the actuation in twist. The cross-sectional geometry is shown in Fig. 6, and the material properties are presented in Table 4. The predicted stiffness coefficients and forcing vector induced by an electric field of -1800 V/1.114×10^{-3} mm are presented in Table 5. Herein, the results corresponding to the

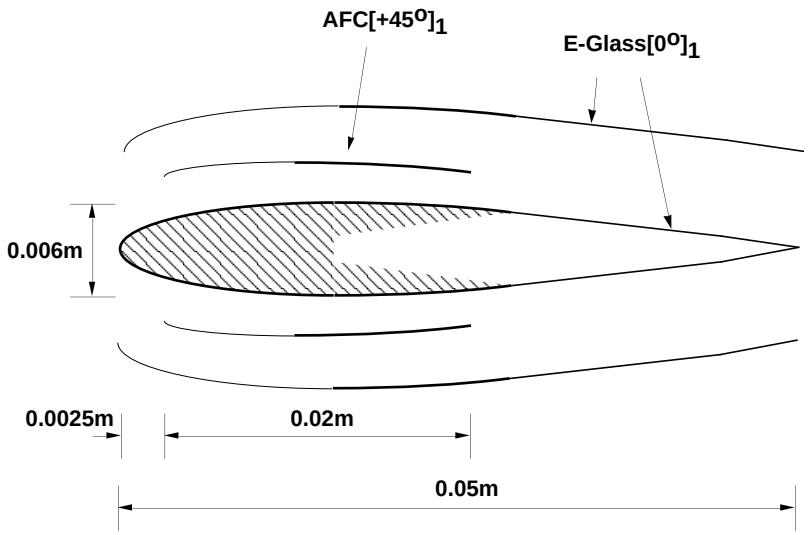

Fig. 6. Single-cell airfoil-shape cross-section beam.

Table 4
Material properties used in the single-cell active beam (Q_{ij} are the laminate reduced stiffnesses of the actuator pack)

E-glass (#120)	E_L	14.8 GPa
	E_T	13.6 GPa
	G_{LT}	6.0 GPa
	ν_{LT}	0.19
	t_{ply}	0.2 mm
AFC (PZT-5H)	Q_{11}	32.8 GPa
	Q_{12}	6.26 GPa
	Q_{22}	17.3 GPa
	Q_{66}	5.5 GPa
	d_{31}	381 pm V^{-1}
	d_{32}	−160 pm V^{-1}
	t_{ply}	0.17 mm

Table 5
Non-zero stiffness (N, N m, N m^2) and forcing vector (N, N m) results for single-cell active beam cross-section – (K_{ij}: 1, extension; 2, torsion; 3, 4, bending)

K_{ij}	Present	Modified Rehfield	Difference (%)
K_{11}	7.552×10^5	7.586×10^5	−0.4
K_{12}	4.541×10^1	4.574×10^1	−0.7
K_{22}	1.848	1.848	0.0
K_{33}	3.996	4.021	−0.6
K_{44}	1.487×10^2	1.490×10^2	−0.2
$F_1^{(a)}$	-3.255×10^1	-4.117×10^1	−20.9
$M_1^{(a)}$	-1.170×10^{-1}	-1.179×10^{-1}	−0.8
$M_3^{(a)}$	-2.557×10^{-3}	-3.192×10^{-3}	−19.8

modified Rehfield model were treated with the condensation procedure explained in the previous section. Furthermore, tension axis was used for the beam reference line due to restrictions on the formulation of the modified Rehfield model (duPlessis and Hagood, 1996). This comes from the original assumption on the passive beam modeling by Rehfield (1985); however, it is not a restriction for the present formulation.

From Table 5, the stiffness matrix reveals that this blade presents extension-shear, extension-torsion and shear-bending couplings, and the results for the stiffness constants show very good agreement between the two formulations. In fact, this level of agreement mainly on the torsional stiffness is a coincidence for this case, due to the lay-up used. (The analytical rationale for such coincidence is discussed in the previous section.) In general, the torsional stiffness will be different since Rehfield's torsional warping only coincides with the asymptotically correct one for laminates with specific characteristics.

Next, one should consider the quantitative aspects of the discrepancies described above. Two different actuation modes are considered here. The first one is mainly twist actuation, responsible for the original $\pm 45°$ orientation of active plies. The twist actuation is obtained through applying the electric field of the same sign as the sign of the angle of the active plies in the upper and lower skin. As a result, a significant amount of actuation is obtained in twist, $M_1^{(a)}$, as well as extension, $F_1^{(a)}$. The latter is considered to result from an extension-twist coupling. The other two components in bending, $M_2^{(a)}$ and $M_3^{(a)}$, are of negligible magnitude. The numerical results are presented in Table 6 (the results of the same twist actuation are also included in Table 5 for completeness), in which a reasonably good agreement is shown for $M_1^{(a)}$. However, a greater discrepancy appears for $F_1^{(a)}$ and further numerical analysis reveals that the second integral in the present formulation plays the main part in the discrepancy. It is also worth noticing that, for $M_2^{(a)}$ and $M_3^{(a)}$,

Table 6
Actuation vector components for the single-cell airfoil-shaped beam

Type of actuation	Analysis model	$F_1^{(a)}$	$M_1^{(a)}$	$M_2^{(a)}$	$M_3^{(a)}$
Twist actuation	Present	-3.255×10^{1}	1.170×10^{-1}	0	-2.557×10^{-3}
	Modified Rehfield	-4.117×10^{1}	1.179×10^{-1}	0	-3.192×10^{-4}
Bending actuation	Present	0	0	-8.350×10^{-2}	0
	Modified Rehfield	0	0	-9.243×10^{-2}	0

the contribution from the second integral in the modified Rehfield model is not significant in this case due to the very thin wall of this airfoil-shaped cross-section.

The cross-sectional results from Table 5 can be used in the 1-D beam analysis that includes the effects of embedded actuation. The corresponding global (1-D) twist results are presented in Fig. 7, where it shows the variation of the blade tip twist as function of applied voltage in the AFC. As one can see, there are no significant differences between both theories. Both predictions are slightly higher than the experimental measurements and this may be partially attributed to the fact that the foam core present in the blade (originally used to facilitate blade manufacturing) has not been modeled by either formulations. However, both theories compare fairly well with the experimental results. If one looks at the extensional deformation due to $F_1^{(a)}$, that would show much higher discrepancies than the ones found in Fig. 7. However, the absolute values of deformation are small and not of practical concern for this example.

Another possible way of actuating the same structure is in bending in which the electric field has opposite signs as compared to the previous case, inducing considerable bending in the flap direction. Table 6 also shows the numerical results of this case, and the only non-zero component is the flapping actuation $M_2^{(a)}$, as expected. However, a discrepancy is also found and this results from the second integral in the present model, similarly to the $F_1^{(a)}$ case described above. The integral including the effect of the thickness is still ineffective in the modified Rehfield model. Experimental data for the bending actuation is not available at this point and future experiments for this blade are necessary to further assess the accuracy of the analyses. However, a numerical estimation of tip flapwise bending deflection shows significant discrepancies between

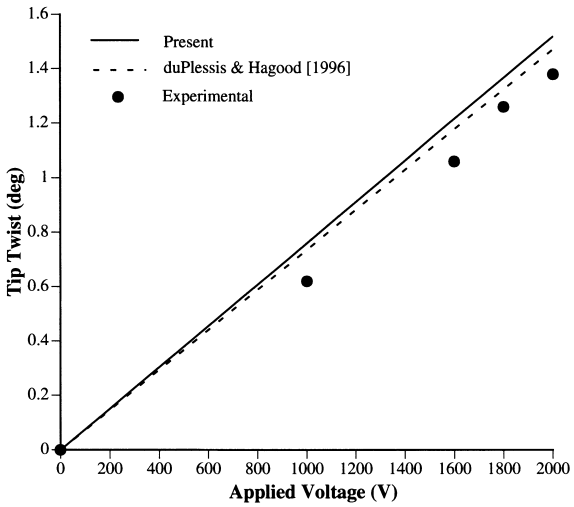

Fig. 7. Tip twist of the single-cell active beam under twist actuation.

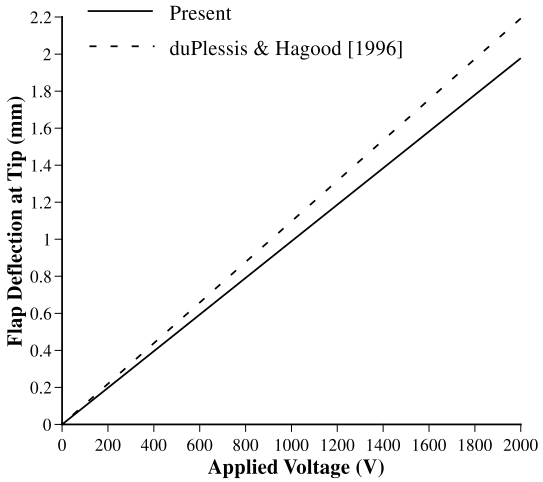

Fig. 8. Flapwise deflection of the single-cell active beam under bending actuation.

the two models even for this weak-actuated beam as shown in Fig. 8. This indicates that discrepancies can be significant on the predicted behavior of an integrally actuated blade response.

In order to quantify the warping, restrained and main transverse shear effects at the cross-sectional modeling for this single-cell active blade, a numerical study was performed among the different cross-sectional analyses. Results are presented in Fig. 9 for the twist distribution along the spanwise coordinate for a constant applied voltage of 1800 V. The results labeled "duPlessis and Hagood (1996)" are from the modified Rehfield model, and they include effects of restrained warping and main transverse shear stiffness, presenting a 7×7 stiffness matrix (although not asymptotically correct for generic layups). The 1-D analysis is linear. The results labeled "6×6 Rehfield and Atılgan (1989), G.E. 1-D" refers to stiffness constants based on the previous formulation but without the restrained warping row and column, reducing the stiffness matrix from the 7×7 to a 6×6 matrix, and the present geometrically exact 1-D formulation (this is not an issue at this point, since the twist is small enough for a linear approximation). Next, the

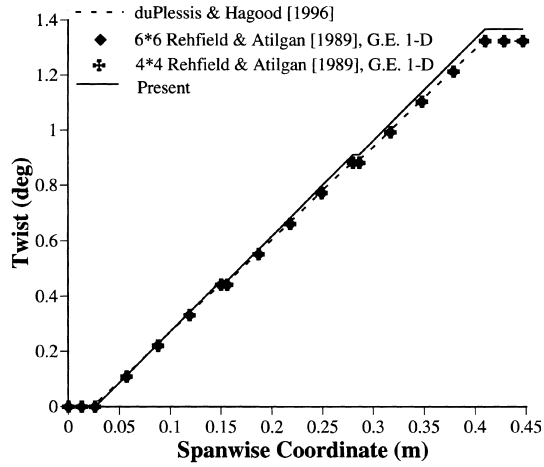

Fig. 9. Single-cell active beam twist distribution.

"4 × 4 Rehfield and Atılgan (1989), G.E. 1-D" has the condensed 4 × 4 stiffness matrix from the previous 6 × 6 formulation, then eliminating the main transverse shear terms. Note that the non-classical coupling effects due to transverse shear have not been neglected but just condensed. All the above are plotted in Fig. 9 along with the present formulation. As one would expect, the restrained warping effects are minimum for a closed-cell beam. For this beam, the main transverse shear effects are also not significant, and a 4 × 4 stiffness formulation is sufficient to account for all the major effects for quasi-static behavior.

4.3. Two-cell CH-47D active blade

A one-sixth Mach-scaled two-cell CH-47D helicopter rotor blade with AFC plies embedded within the front D-spar (Rodgers and Hagood, 1998a) is used to study the actuation constants and global blade structural behavior of a multi-cell active beam. Two configurations of part of that blade running from the root to 0.54 radius have been built and tested at MIT. The first involves only the front D-spar, and the second includes the fairing as well, this making the cross-section of the blade a two-cell configuration. Two analytical predictions using the modified Rehfield model (duPlessis and Hagood, 1996), which is originally restricted to single-cell beams, and experimental data from the prototype blade are compared with the results from the present formulation. The cross-section and spanwise design of CH-47D active blade are shown in Fig. 10, along with the detailed layup. Even though not explicitly presented there, both cells are filled with a Rohacell foam for manufacturing reasons, and that core material is not modeled in the present formulation.

First, consider the stiffness and actuation constants for this blade. Analytical comparison of the Modified Rehfield analysis with the present formulation is summarized in Table 7 where the cross-sectional analysis results consider only the front D-spar component that can be modeled as a single-cell cross-section. It is noticed that the components related to the torsional deformation, such as torsional stiffness K_{22} and twisting actuation moment $M_1^{(a)}$, are in good agreement with each other. Therefore, this example is another case in which both analytical models give coinciding results for these components.

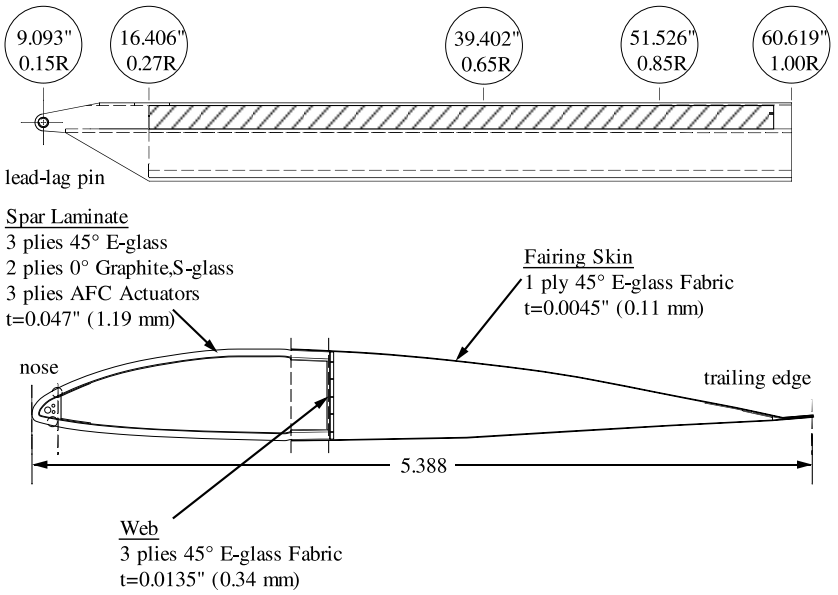

Fig. 10. Schematic diagram of the complete CH-47D active blade section (Rodgers and Hagood, 1998b).

Table 7
Non-zero stiffness (N, Nm, Nm^2) and forcing vector (N, Nm) results for CH-47D D-spar only – (K_{ij}: 1, extension; 2, torsion; 3, 4, bending)

	Present	Modified Rehfield	Difference (%)
K_{11}	4.662×10^6	4.663×10^6	−0.01
K_{12}	-2.947×10^2	-2.948×10^1	−0.02
K_{22}	8.862×10^1	8.862×10^1	0.0
K_{33}	1.793×10^2	1.710×10^2	+4.8
K_{44}	1.145×10^3	1.142×10^3	+0.28
$F_1^{(a)}$	7.139×10^1	6.784×10^1	+4.9
$M_1^{(a)}$	2.496	2.496	−0.02

Table 8
Non-zero stiffness (N, Nm, Nm^2) and forcing vector (N, Nm) results for CH-47D active blade section (front D-spar + fairing) – (K_{ij}: 1, extension; 2, torsion; 3, 4, bending)

	Present	Modified Rehfield + ad hoc corrections	Difference (%)
K_{11}	5.171×10^6	5.989×10^6	−13.6
K_{12}	-3.012×10^2	-2.948×10^2	+2.2
K_{22}	9.872×10^1	1.085×10^2	−9.1
K_{33}	1.908×10^2	1.818×10^2	+4.9
K_{44}	4.390×10^3	3.923×10^3	+11.9
$F_1^{(a)}$	8.442×10^1	6.784×10^1	+24.4
$M_1^{(a)}$	2.362	2.312	+2.1

Next, consider the entire cross-section, i.e., front D-spar and fairing. Cross-sectional results are presented in Table 8. The results associated with "modified Rehfield + ad hoc corrections" are obtained by combining the analysis results considering the front D-spar and some "appropriate" stiffness constants corresponding to the remaining components like skin plies of the fairing, core material, and tungsten weights that are inserted at the nose section. These corrections were introduced by Boeing Helicopter engineers based on their experience, and it is reported in Rodgers and Hagood (1998b). The correlation is not as good as in the previous cases due to a more complex cross-sectional construction and the limitation of the present analysis to thin-walled modeling. A more generic cross-sectional representation that captures the core material and internal details of the construction (like the one provided by VABS-A (Cesnik and Ortega-Morales, 1999)) is required for improved accuracy.

Finally, consider the 1-D twist results under actuation for both the D-spar and for the complete cross-section (including fairing). The twist actuation rates are summarized in Table 9. The "present" results included the cross-sectional and beam analyses presented here. For the "modified Rehfield" results, only the D-spar case is available, since its limitation to single-cell analysis. The "modified Rehfield + ad hoc corrections" results are a combination of the single-cell analysis and stiffness corrections (no corrections on the actuation constants, even though they are function of the stiffness as well) provided by Boeing engineers and reported in Rodgers and Hagood (1998b). For the D-spar only, the result from the present formulation and the "modified Rehfield" analysis of duPlessis and Hagood (1996) are numerically identical. This is not a surprise considering the 2-D results presented in Table 7. The "ad hoc" corrections to the "modified Rehfield" analysis include mainly the effects of the ballast weights at the nose. These corrections improve the correlation with the experimental result from an overprediction of 27% down to 14%, however, no asymptotic consistency is present on this process. Now, for the complete section (D-spar and fairing), the present formulation still presents the same relative level of correlation with the experi-

Table 9
Twist actuation rate comparison for CH-47D active blade section (D-spar only and full cross-section: analyses and experiment)

	D-spar only		D-spar + fairing	
	Twist actuation ($°m^{-1}$)	Difference (%)	Twist actuation ($°m^{-1}$)	Difference (%)
Present	3.13	27	2.65	28
Modified Rehfield	3.13	27	–	–
Modified Rehfield + ad hoc corrections	2.81	14	2.55	24
Experiment	2.46	–	2.06	–

mental data. The simple "modified Rehfield" result is not available for the complete section due to the basic limitation on the formulation. The "modified Rehfield + ad hoc corrections" result shows the closer correlation with the experimental measurement, but it is now about the same magnitude as the present formulation, where the effects of the ballast weight or the core material have not been modeled. This change on the error margin is characteristic of non-asymptotical formulations. Some of the discrepancies found between the present formulation and the experimental data are primarily caused by the limited capability of the present analysis to model minor structural members like foam cores and ballast weights. Also, the experimental twist actuation of the CH-47D active blade may be lower than originally expected from a flawless construction. After slicing the CH-47D blade and examining the inner structure, it turned out that some defects developed within the blade during its manufacturing and may have partially degraded its actuation performance (Rodgers and Hagood, 1998b).

5. Conclusion

An asymptotical formulation for analyzing multi-cell composite helicopter rotor blades with integral anisotropic active plies was presented for the first time. The analysis derived in this paper consists of two parts: a linear two-dimensional analysis over the cross-section, and a geometrically non-linear (beam) analysis along the blade span. A numerical study was conducted to validate the two-cell blade analysis and the piezoelectric actuation change in the beam constitutive relation. Finite-element-based cross-section analysis and other closed-form formulation were used for that study. Comparison of the present asymptotically correct analytical and numerical results is conducted against a popular assumed-displacement field cross-sectional analysis. It is shown that qualitative discrepancies are found on the expressions for the active forcing vector components, and numerical studies show that those discrepancies can indeed be significant on the predicted behavior of the one-dimensional blade. Experimental data obtained at MIT for active model blades were used to validate the present formulation. As shown in the results, a very good correlation with experimental data was obtained with the present formulation. This formulation is now being applied to design an active twist rotor with active fiber composites for aeroelastic tests at the Transonic Dynamics Tunnel at NASA Langley.

Acknowledgements

This work was sponsored in part by the US Army Vehicle Technology Center, at NASA Langley Research Center. The technical monitors are Mr. Paul H. Mirick and Dr. W. Keats Wilkie.

Appendix A

A.1. Cross-sectional formulation

In the first part of this appendix, explicit expressions are reported for some of the relevant variables used in the development, including the stiffness coefficients K_{ij} which have some corrections from the original ones presented in Badir (1995):

$$
\begin{aligned}
K_{11} &= \oint \left(A - \frac{B^2}{C}\right) \mathrm{d}s - 4a_3 \oint_{\mathrm{I}} \frac{B}{C}\,\mathrm{d}s - 4a_4 \oint_{\mathrm{II}} \frac{B}{C}\,\mathrm{d}s,\\
K_{12} &= 4a_1 \oint_{\mathrm{I}} \frac{B}{C}\,\mathrm{d}s + 4a_2 \oint_{\mathrm{II}} \frac{B}{C}\,\mathrm{d}s,\\
K_{13} &= -\oint \left(A - \frac{B^2}{C}\right) z\,\mathrm{d}s - 4a_7 \oint_{\mathrm{I}} \frac{B}{C}\,\mathrm{d}s - 4a_8 \oint_{\mathrm{II}} \frac{B}{C}\,\mathrm{d}s,\\
K_{14} &= -\oint \left(A - \frac{B^2}{C}\right) y\,\mathrm{d}s - 4a_3 \oint_{\mathrm{I}} \frac{B}{C}\,\mathrm{d}s - 4a_4 \oint_{\mathrm{II}} \frac{B}{C}\,\mathrm{d}s,\\
K_{22} &= -4a_1 A_{e\mathrm{I}} - 4a_2 A_{e\mathrm{II}},\\
K_{23} &= 4a_7 A_{e\mathrm{I}} + 4a_8 A_{e\mathrm{II}},\\
K_{24} &= -4a_5 A_{e\mathrm{I}} - 4a_6 A_{e\mathrm{II}},\\
K_{33} &= \oint \left(A - \frac{B^2}{C}\right) z^2\,\mathrm{d}s + 4a_7 \oint_{\mathrm{I}} \frac{B}{C} z\,\mathrm{d}s + 4a_8 \oint_{\mathrm{II}} \frac{B}{C} z\,\mathrm{d}s,\\
K_{34} &= -\oint \left(A - \frac{B^2}{C}\right) yz\,\mathrm{d}s - 4a_5 \oint_{\mathrm{I}} \frac{B}{C} z\,\mathrm{d}s - 4a_6 \oint_{\mathrm{II}} \frac{B}{C} z\,\mathrm{d}s,\\
K_{44} &= \oint \left(A - \frac{B^2}{C}\right) y^2\,\mathrm{d}s + 4a_5 \oint_{\mathrm{I}} \frac{B}{C} y\,\mathrm{d}s + 4a_6 \oint_{\mathrm{II}} \frac{B}{C} y\,\mathrm{d}s,
\end{aligned}
$$

where

$$
\begin{aligned}
a_1 &= -\frac{c_3}{c_1},\\
a_2 &= \frac{(b_1 + b_2)a_1 + b_4}{b_2},\\
a_3 &= -\frac{c_2}{c_1},\\
a_4 &= \frac{(b_1 + b_2)c_4 + b_3}{b_2},\\
a_5 &= \frac{b_5 \oint_{\mathrm{I}} by\,\mathrm{d}s + b_2 d_1}{e_1},\\
a_6 &= \left(\frac{b_1 + b_2}{b_2}\right) d_3 - \frac{\oint_{\mathrm{I}} by\,\mathrm{d}s}{b_2},\\
a_7 &= \frac{b_5 \oint_{\mathrm{I}} bz\,\mathrm{d}s + b_2 d_2}{e_1},\\
a_8 &= \left(\frac{b_1 + b_2}{b_2}\right) d_4 - \frac{\oint_{\mathrm{I}} bz\,\mathrm{d}s}{b_2},
\end{aligned}
$$

and

$$
\begin{aligned}
b &= -2\frac{B(s)}{C(s)},\\
b_1 &= 4\int_0^{s_1} c(s)\,\mathrm{d}s,\\
b_2 &= 4\int_{s_1}^{s_2} c(s)\,\mathrm{d}s,\\
b_3 &= \oint_{\mathrm{I}} b(s)\,\mathrm{d}s,\\
b_4 &= -2A_{e\mathrm{I}},\\
b_5 &= 4\int_{s_2}^{s_3} c(s)\,\mathrm{d}s,\\
b_6 &= \oint_{\mathrm{II}} b(s)\,\mathrm{d}s,\\
b_7 &= -2A_{e\mathrm{II}},\\
c &= -2\frac{1}{C(s)},\\
c_1 &= b_1 + \frac{(b_1+b_2)b_5}{b_2},\\
c_2 &= b_3 + b_6 + \frac{b_3 b_5}{b_2},\\
c_3 &= b_4 + b_7 + \frac{b_4 b_5}{b_2},\\
d_1 &= \oint_{\mathrm{I+II}} by\,\mathrm{d}s,\\
d_2 &= \oint_{\mathrm{I+II}} bz\,\mathrm{d}s,\\
d_3 &= \frac{b_5 \oint_{\mathrm{I}} by\,\mathrm{d}s + b_2 d_1}{e_1},\\
d_4 &= \frac{b_5 \oint_{\mathrm{I}} bz\,\mathrm{d}s + b_2 d_2}{e_1},\\
e_1 &= b_1 b_2 + (b_1+b_2)b_5.
\end{aligned}
$$

A.2. 1-D blade formulation

Consider the expressions of the element functions (Shang and Hodges, 1995) presented in Eq. (32) and modified due to the inclusion of the piezoelectric forcing vector. If one writes the inverse of the constitutive relation, Eq. (28) as

$$
\begin{Bmatrix} \gamma \\ \kappa \end{Bmatrix} = \begin{bmatrix} r & t \\ t^{\mathrm{T}} & s \end{bmatrix} \begin{Bmatrix} F_{\mathrm{B}} + F_{\mathrm{B}}^{(\mathrm{a})} \\ M_{\mathrm{B}} + M_{\mathrm{B}}^{(\mathrm{a})} \end{Bmatrix},
$$

then the modified element functions can be written explicitly as

$$
\begin{aligned}
f_{\psi_i} &= -C^{\mathrm{T}}C^{\mathrm{ab}}M_i - \frac{\Delta l_i}{2}C^{\mathrm{T}}C^{\mathrm{ab}}\left[e_1 + \left\{r\left(F_i + F_i^{(\mathrm{a})}\right)\widetilde{+\,t}\left(M_i + M_i^{(\mathrm{a})}\right)\right\}\right]F_i + \cdots,\\
f_{F_i} &= u_i - \frac{\Delta l_i}{2}\left[C^{\mathrm{T}}C^{\mathrm{ab}}\left(e_1 + \left\{r\left(F_i + F_i^{(\mathrm{a})}\right) + t\left(M_i + M_i^{(\mathrm{a})}\right)\right\}\right) - C^{\mathrm{ab}}e_1\right],\\
f_{M_i} &= \theta_i - \frac{\Delta l_i}{2}\left(\Delta + \frac{\widetilde{\theta}_i}{2} + \frac{\theta_i\theta_i^{\mathrm{T}}}{4}\right)C^{\mathrm{ab}}\left\{t^{\mathrm{T}}\left(F_i + F_i^{(\mathrm{a})}\right) + s\left(M_i + M_i^{(\mathrm{a})}\right)\right\},\\
f_{\psi_{i+1}} &= C^{\mathrm{T}}C^{\mathrm{ab}}M_i - \frac{\Delta l_i}{2}C^{\mathrm{T}}C^{\mathrm{ab}}\left[e_1 + \left\{r\left(F_i + F_i^{(\mathrm{a})}\right)\widetilde{+\,t}\left(M_i + M_i^{(\mathrm{a})}\right)\right\}\right]F_i + \cdots,\\
f_{F_{i+1}} &= -u_i - \frac{\Delta l_i}{2}\left[C^{\mathrm{T}}C^{\mathrm{ab}}\left(e_1 + \left\{r\left(F_i + F_i^{(\mathrm{a})}\right) + t\left(M_i + M_i^{(\mathrm{a})}\right)\right\}\right) - C^{\mathrm{ab}}e_1\right],\\
f_{M_{i+1}} &= -\theta_i - \frac{\Delta l_i}{2}\left(\Delta + \frac{\widetilde{\theta}_i}{2} + \frac{\theta_i\theta_i^{\mathrm{T}}}{4}\right)C^{\mathrm{ab}}\left\{t^{\mathrm{T}}\left(F_i + F_i^{(\mathrm{a})}\right) + s\left(M_i + M_i^{(\mathrm{a})}\right)\right\}.
\end{aligned}
$$

References

Badir, A.M., 1995. Analysis of two-cell composite beams. Proceedings of the 36th AIAA Structures, Structural Dynamics and Materials Conferences, New Orleans, AIAA 95-1208-CP.

Barrett, R., 1990. Intelligent rotor blade and structures development using directionally attached piezoelectric crystals. M.S. Thesis, University of Maryland, College Park, Maryland.

Bent, A.A., Hagood, N.W., 1997. Piezoelectric fiber composites with interdigitated electrodes. Journal of Intelligent Material Systems and Structures 8 (11), 903–919.

Berdichevsky, V.L., 1979. Variational-asymptotical method of shell theory construction. PMM 43 (4), 664–687.

Berdichevsky, V.L., Armanios, E., Badir, A.M., 1992. Theory of anisotropic thin-walled closed-cross-section beams. Composites Engineering 2 (5–7), 411–432.

Cesnik, C.E.S., Hodges, D.H., 1997. VABS: A new concept for composite rotor blade cross-sectional modeling. Journal of American Helicopter Society 42 (1), 27–38.

Cesnik, C.E.S., Ortega-Morales, M., 1999. Active composite beam cross-sectional modeling–stiffness and active force constants. Proceedings of the 40th AIAA Structures, Structural Dynamics and Materials Conferences. St. Louis, Missouri, AIAA-99-1548.

Cesnik, C.E.S., Shin, S., Wilkie, W.K., Wilbur, M.L., Mirick, P.H., 1999. Modeling, design, and testing of the NASA/Army/MIT active twist rotor prototype blade. Proceedings of American Helicopter Society 55th Annual Forum, Montreal, Canada, 25–27 May.

Chen, P.C., Chopra, I., 1993. A feasibility study to build a smart rotor: induced-strain actuation of airfoil twisting using piezoceramic crystals. Proceedings of the Society of Photo-Optical and Instrumentation Engineering vol. 1917. San Diego, California, pp. 238–254.

Chen, P.C., Chopra, I., 1997. Hover testing of smart rotor with induced-strain actuation of blade twist. AIAA Journal 35 (1), 6–16.

duPlessis, A.J., Hagood, N.W., 1996. Modeling and experimental testing of twist actuated single cell composite beams for helicopter rotor blade control. AMSL Report 96-1, Massachusetts Institute of Technology.

Friedmann, P.P., 1997. The promise of adaptive materials for alleviating aeroelastic problems and some concerns. Proceedings of Innovation in Rotorcraft Technology. Royal Aeronautical Society London, United Kingdom, 24–25 June, pp. 10.1–10.16.

Hodges, D.H., 1990. A mixed variational formulation based on exact intrinsic equations for dynamics of moving beams. International Journal of Solids and Structures 26 (11), 1253–1273.

Hodges, D.H., Atilgan, A.R., Cesnik, C.E.S., Fulton, M.V., 1992. On a simplified strain energy function for geometrically nonlinear behavior of anisotropic beams. Composites Engineering 2 (5–7).

Jaffe, B., Cook, W.R., Jaffe, H., 1971. Piezoelectric Ceramics. Academic Press, New York.

Jones, R.M., 1975. Mechanics of Composite Materials. Hemisphere, New York.

Loewy, R.G., 1997. Recent developments in smart structures with aeronautical applications. Proceedings of the 37th Israel Annual Conference on Aerospace Sciences. 26–27 February.

Rehfield, R.W., 1985. Design analysis methodology for composite rotor blades. Proceedings of the Seventh DoD/NASA Conference on Fibrous Composites in Structural Design. Denver, CO, Grant NAG-2-238.

Rehfield, R.W., Atılgan, A.R., 1989. Shear center and elastic axis and their usefulness for composite thin-walled beams. Proceedings of the American Society for Composites, Fourth Technical Conference. Blacksburg, Virginia, pp. 179–188.

Rodgers, J.P., Hagood, N.W., 1998a. Preliminary mach-scale hover testing of an integral twist-actuated rotor blade. Proceedings of the Society of Photo-Optical and Instrumentation Engineering. vol. 3329, pp. 291–308.

Rodgers, J.P., Hagood, N.W., 1998b. Development of an integral twist-actuated rotor blade for individual blade control. AMSL Report 98-6, Massachusetts Institute of Technology, October.

Rodgers, J.P., Hagood, N.W., Weems, D.B., 1997. Design and manufacture an integral twist-actuated rotor blade. Proceedings of the 38th AIAA/ASME/AHS/ASC Structures, Structural Dynamics and Materials Conferences. Kissimmee, Florida, AIAA Paper No. 97–1264.

Shang, X., Hodges, D.H., 1995. Aeroelastic stability of composite rotor blade in hover. Proceedings of the 36th Structures, Structural Dynamics and Materials Conferences. New Orleans, Louisiana, 10–12 April.

Smith, E.C., Chopra, I., 1990. Formulation and evaluation of an analytical model for composite box beams. Proceedings of the 31st AIAA/ASME/AHS/ASC Structures, Structural Dynamics and Materials Conferences April, AIAA Paper No. 90-0962-CP.

Song, O., Librescu, L., 1993. Vibrational behavior of rotating helicopter blades incorporating adaptive capabilities, Proceedings of SPIE Smart Structures and Materials Conference. vol. 1917, Part 1.

Volovoi, V.V., Hodges, D.H., Cesnik, C.E.S., Popescu, B., 1999. Assessment of beam modeling methods for rotor blade applications. Proceedings of the 55th American Helicopter Society Annual Forum. Montreal, Canada, 25–27 May.

Wilkie, W., Belvin, W., Park, K.C., 1996. Aeroelastic analysis of helicopter rotor blade incorporating anisotropic piezoelectric twist actuator. ASME 1996 World Congress and Exposition.